Geometric and Tooth Contact Analysis of the Areas and Perimeters, on the Archimedean Worm Wheels depending on the Modification of the Axial Module

Sándor Bodzás[1], Gyöngyi Szanyi[2]

[1]Department of Mechanical Engineering, University of Debrecen
[2]Department of Basic Technical Studies, University of Debrecen
4031 Debrecen, Ótemető u. 2-4, Hungary
*E-mail: [1]bodzassandor@eng.unideb.hu, [2]szanyi.gyongyi@science.unideb.hu

Abstract: The goal of this study is to determine the correlation between the modification of the axial module and the received mechanical parameters on the teeth, of the worm gear. We analyze the areas and perimeters of the impressions on the teeth of the worm gear comparing the module changing. Six types of Archimedean worm gear drives are designed by the modification of the axial module to analyze the mechanical parameters between the connecting teeth of the pinion and the gear. After that, computer aided models are generated. These pairs are loaded with the same torque, to analyze the mechanical parameters on the tooth contact zone. Due to the geometric establishment, three teeth of the worm wheels are connected with the worm surface, at the same time, that is why these teeth are analyzed continuously. We approach the kinematic impressions on the surface of the worm wheel, by polygon method, to get percentage ratios between the areas and perimeters of the overall profile and the tooth contact zone, on the worm wheel, for each connecting tooth. We also determine the correlation between the axial module and the analyzed mechanical parameters, assuming average values, on the contact surfaces.

Keywords: worm; worm wheel; module; teeth; stress; deformation

1 Introduction

Worm gear drives are widely used for different engineering constructions, they provide high transmission ratios and perpendicular shaft positions, between the elements. More teeth are connected at the same time, this is why higher torque can be transferred, than in the case of spur gears and bevel gears [1, 2, 4-9, 20-22, 24].

The aim of the TCA is to analyze the mechanical parameters of the gear pairs in the tooth connection based on different loads. It is a part of finite element analysis where the tooth connection can be analyzed. Consequently, it is possible to simulate

the working conditions of the gear pairs. If we get non-required results, it is possible to mediate the design process, before the real manufacturing and the industrial working begins[7] [23].

Although the manufacturing process of the worm wheel is complicated, it can be generated by direct motion mapping. It means the geometry of the worm defines the cutting tool, which is called hob, which manufactures the teeth of the worm wheel [1, 4, 25-27]. Geometrically, the worm and the hob are the same. The difference between them are the addendum and the tooth width. We should provide clearances during the tooth connection to avoid heat deformations [1, 4, 25-27].

F. L. Litvin found the mathematical processes needed to determine and optimize the tooth contact areas in case of different gears. He designed special drives for different companies. His research group developed computer aided software for the geometrical designing and the localization of the contact area on toothed gears [6, 7, 23].

A. Fuentes Aznar and his research group deal with TCA which contains geometric design, CAD and FEM for standardized gear drives and special connecting elements [7]. The aim of the TCA is to determine the mechanical parameters on the tooth contact zone by different load forces and torques depending on the material type [7] [23].

I. Dudás researches the manufacturing development of the different worm gear drives. He also analyzes these elements by mathematical way to provide the correct connection and manufacturing process for them. The development stages of the grinding processes are important for the assurance of the better connection and the reduction of the wearing between the kinematic pairs [4].

T. Bercsey analyzed the connection of the globoid worm and hyperbolic gear. On the other hand, he proved the application of the kinematic method in case of toroidal gears [2] [3].

I. Sz. Krivenko invented the cylindrical worm gear drives having an arched profile in the axial section. Based on his experience, he recommended a certain design process for this construction. The advantage of this geometry is the convex-concave teeth connection, which results in better contact lines and areas, than in case of linear profile [8].

V. Goldfarb works on the geometrical development of spiroid- and cylindrical worm gears by mathematical and constructional way. He analyzes the contact mechanical parameters by FEM for the geometrical localization [13] [14].

Paper [9] presents the matrix - vectorial mathematical model of the double worm-face gear with cylindrical worm and a graphical modelling which is based on the specific geometrical characteristics accomplished by means of the Autodesk Inventor 3D modelling program.

Paper [10] presents a computation method of worm gears with Archimedean and involute worms when engagement correction is presented, based on the contact pressures and wear of tooth of the wheel, as well as the gear life and the sliding speed in the engagement.

Paper [11] illustrates a machining method of large-sized cylindrical worm gears with Niemann profiles using a computer numerical control (CNC) machining center is introduced. The tooth contact pattern and transmission errors of large-sized worm gear pair with Niemann profiles are analyzed before machining of the worm and worm wheel. After that, the machining conditions of the worm is determined by calculating each offset distance between the worm axis and the center axis of the end mill, and then the worm is machined by swarf cutting. That means machining by the side surface of the end mill.

Paper [12] describes the results of the machine tool setting errors of the worm gear hobbing and its effects of the shaft misalignments of the worm gear set on the interference.

Paper [15] presents the investigation of the meshing theory for the mismatched ZC1 worm drive. The contact endpoints, the datum point, and the internal instantaneous contact points are all determined by solving their corresponding nonlinear equation sets iteratively. The numerical results of the relative principal curvature, the transmission error, and the drive ratio error of the worm drive are all obtained.

Paper [16] presents the geometric and kinematic design of spur gears, bevel gears, worm gears, planetary gears and face gear drives. It contains formulas for the geometric design and recommends manufacturing strategies for these gear pairs.

Paper [17] presents the geometric interference of cylindrical worm gear drives using an oversized hob to cut the worm gear. The instantaneous line contact of a fully conjugated gear set becomes an instantaneous point contact when an oversized hob is used.

Paper [18] presents the increasing requirements of high-precision and high bearing capacity in industrial robot and aerospace technology, a novel point-contact hourglass worm drive consisting of an involute helical beveloid (IHB) gear and an oblique planar enveloping (OPE) hourglass worm.

Paper [29] presents a methodology for precisely calculating the tooth thickness of cylindrical worm gear, which is expounded in great detail, with the worm gear in the toroidal surface enveloping cylindrical worm pair, as a sample. This method can calculate the tooth thickness in any cross section of cylindrical worm gear, and it is universal for cylindrical worm gears.

Paper [30] presents an overall process of worm gear drives where all the steps from the idea to the final product are performed integrated on the computer. It is also important to reduce the dynamic loads by different methods. Dynamic Simulation in Autodesk Inventor Professional was chosen to analyze the dynamic operating

conditions of a project in a complete operating cycle. This simulation provides analysis tools that allow the evaluation of product performance in a 3D environment.

Paper [31] presents a meshing performance analysis which makes it possible to use the plane meshing theory and the space enveloping principle to analyze involute worm and helical gear drive. The meshing relationship between the involute worm and the counterpart rack, as well as the counterpart rack and the helical gear are shown, and the computational model of contact ratio and contact ellipse are obtained through the counterpart rack.

2 Mathematical Approach of Archimedean Worm

The worm surface is generated by such cutting tool which has straight-lined blade. This cutting edge is situated in the axial section of the worm [4, 6, 7, 20, 26-28]. The generating lines are in coordinate system C_p, which is connected to the edge of the tool. This coordinate system does rotational and linear motion at the same time, which generates the helical surface of the worm [4, 6, 7, 20, 26-28] on the C_{1R} coordinate system (Figure 1). The transformation matrix between the C_P and C_{1R} systems is:

$$M_{1R,p} = \begin{bmatrix} cos\theta & -sin\theta & 0 & 0 \\ sin\theta & cos\theta & 0 & 0 \\ 0 & 0 & 1 & \pm p \cdot \theta \\ 0 & 0 & 0 & 1 \end{bmatrix} \tag{1}$$

In case of right-hand worm, Surface side I can be calculated (Figure 1.a.):

$$\left.\begin{aligned} x_{1RI} &= \eta \cdot cos\alpha_{ax} \cdot cos\theta \\ y_{1RI} &= \eta \cdot cos\alpha_{ax} \cdot sin\theta \\ z_{1RI} &= -\eta \cdot sin\alpha_{ax} + \left(r_0 \cdot tan\alpha_{ax} - \frac{p_x - s_{ax1}}{2}\right) + p \cdot \theta \end{aligned}\right\} \tag{2}$$

The generated surface on the C_{1R} coordinate system is after giving a helical motion for the C_P coordinate system (Figure 1.b.):

$$\vec{r}_{1R}(\eta, \theta) = M_{1R,p}(\theta) \cdot \vec{r}_p(\eta) \tag{3}$$

Based on Figure 1. the unit normal vector is [7]:

$$\vec{n}_{1R}(\eta, \theta) = \frac{\partial \vec{r}_{1R}}{\partial \eta} \times \frac{\partial \vec{r}_{1R}}{\partial \theta} \tag{4}$$

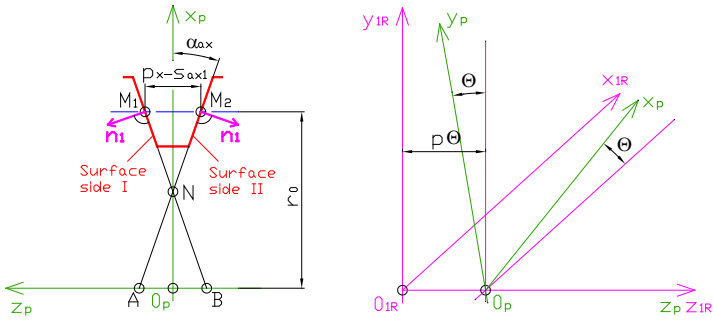

Figure 1
Geometry of the cutting edge (a) and coordinate transformation (b)

The surface unit normal vector of the Surface side I is after the (4) cross product:

$$\vec{n}_{1RI}(\eta,\theta) = (p \cdot sin\,\theta + \eta \cdot sin\alpha_{ax} \cdot cos\,\theta) \cdot \vec{\imath}$$
$$-(p \cdot cos\theta - \eta \cdot sin\alpha_{ax} \cdot sin\,\theta) \cdot \vec{\jmath} + \eta \cdot cos\alpha_{ax} \cdot \vec{k} \tag{5}$$

In case of right-hand worm, the Surface side II can be calculated (Figure 1.b.):

$$\left.\begin{aligned} x_{1RII} &= \eta \cdot cos\alpha_{ax} \cdot cos\theta \\ y_{1RII} &= \eta \cdot cos\alpha_{ax} \cdot sin\theta \\ z_{1RII} &= \eta \cdot sin\alpha_{ax} - \left(r_0 \cdot tan\alpha_{ax} - \frac{p_x - s_{ax1}}{2}\right) + p \cdot \theta \end{aligned}\right\} \tag{6}$$

The surface unit normal vector of the Surface side II is after the (4) cross product:

$$\left.\begin{aligned} &\vec{n}_{1RII}(\eta,\theta) = (p \cdot sin\,\theta - \eta \cdot sin\alpha_{ax} \cdot cos\,\theta) \cdot \vec{\imath} \\ &-(p \cdot cos\theta + \eta \cdot sin\alpha_{ax} \cdot sin\,\theta) \cdot \vec{\jmath} + \eta \cdot cos\alpha_{ax} \cdot \vec{k} \end{aligned}\right\} \tag{7}$$

If y_{1R}=0, the equations of the two sections are x_{1R}= x_{1R}(η) and z_{1R}= z_{1R}(η):

$$\left.\begin{aligned} x_{1R} &= \eta \cdot cos\alpha_{ax} \\ y_{1R} &= 0 \\ z_{1R} &= \eta \cdot sin\alpha_{ax} - \left(r_0 \cdot tan\alpha_{ax} - \frac{p_x - s_{ax1}}{2}\right) \end{aligned}\right\} \tag{8}$$

$$\left.\begin{aligned} x_{1R} &= -\eta \cdot cos\alpha_{ax} \\ y_{1R} &= 0 \\ z_{1R} &= \eta \cdot sin\alpha_{ax} - \left(r_0 \cdot tan\alpha_{ax} - \frac{p_x - s_{ax1}}{2}\right) + p \cdot \pi \end{aligned}\right\} \tag{9}$$

The contact points between the connecting elements can be calculated by the Connection I Statement [6] [7]:

$$\overrightarrow{n_{1R}} \cdot \overrightarrow{v_{1R}} = 0 \tag{10}$$

The formula (10) can also be used to determinate surface of the worm wheel if the worm surface is known [1, 4-7, 22, 23, 25, 27]. The detailed formulas can be programed if we do not have gear designer software which can do the modelling

process. Using of the detailed formulas an own developed software can be made on an arbitrary programing language to prepare the CAD models of the worm and the worm wheel.

3 Design and Modelling Process

Based on the recommendations of the references [4-8, 13, 14, 16, 20, 21, 27] six types of Archimedean worm gear drives are designed by different axial modules. All the other input parameters are unchanged (f', c^*, r', z_1, z_2, L, b_2, α_n, j).

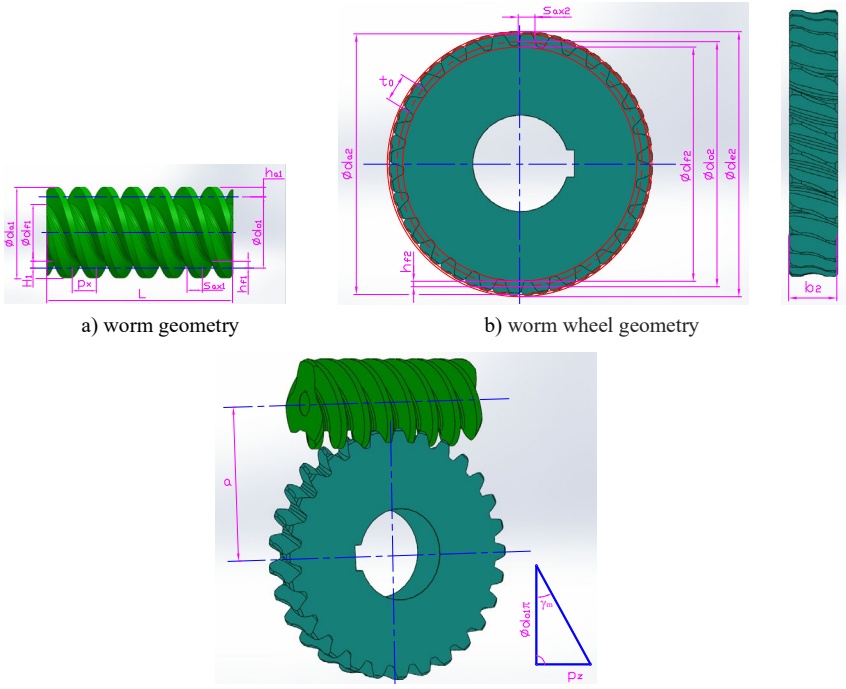

a) worm geometry b) worm wheel geometry

c) assembled model

The geometrical parameters of the worm and the worm wheel

Table 1
The calculated parameters of the designed worm gear drives

The parameters of the worm gear drive	**I.**	**II.**	**III.**	**IV.**	**V.**	**VI.**
Axial module (m_{ax}) [mm]	6.5	7	8	9	10	11
Diametral pitch (p_d) [mm]	3.907	3.628	3.175	2.822	2.54	2.309
Normal diametral pitch (p_{dn}) [mm]	4.022	3.751	3.314	2.978	2.712	2.497
Normal module (m_n) [mm]	6.315	6.77	7.662	8.527	9.363	10.168
Worm lead of thread (p_x) [mm]	61.3	66	75.4	84.8	94.2	103.7
Circular pitch of the worm-wheel (t_0) [mm]	20.4	22	25.1	28.3	31.4	34.6
Lead angle (γ_m) [mm]	13.7	14.7	16.7	18.6	20.6	22.4
Addendum coefficient (f')	1					
Clearance coefficient (c*)	0.2					
Fillet coefficient (r')	0.3					
Number of threads (z_1)	3					
Number of teeth of the worm-wheel (z_2)	28					
Direction of the wheel	right hand					
Pitch diameter of the worm (d_{01}) [mm]	80					
Pitch diameter of the worm-wheel (d_{02}) [mm]	182	196	224	252	280	308
Outside diameter of the worm (d_{a1}) [mm]	93	94	96	98	100	102
Outside diameter of the worm-wheel (d_{a2}) [mm]	199.8	214.9	245.1	275.3	305.5	335.7
Center distance (a) [mm]	131	138	152	166	180	194
Face width of the worm-wheel (b_2) [mm]	50					
Worm length (L) [mm]	200					
Pressure angle (α_{ax}) [°]	20.5	20.6	20.8	21	21.2	21.5
Normal pressure angle (α_n) [°]	20					
Addendum of the worm (h_{a1}) [mm]	6.5	7	8	9	10	11
Addendum of the worm-wheel (h_{a2}) [mm]	6.5	7	8	9	10	11
Dedendum of the worm (h_{f1}) [mm]	7.6	8.2	9.3	10	11.7	12.8
Dedendum of the worm-wheel (h_{f2}) [mm]	7.6	8.2	9.3	10.5	11.7	12.8

Tooth thickness of the worm (S_{ax1}) [mm]	10.2	11	12.6	14.1	15.7	17.3
Tooth thickness of the worm-wheel (S_{ax2}) [mm]	9.2	10	11.6	13.1	14.7	16.3
Fillet radius (r) [mm]	1.9	2.1	2.4	2.7	3	3.3
Backlash (j) [mm]	1					
Transmission ratio (i)	3/28					
Diameter ratio (q)	10					11

4 Analysis of the Contact Surfaces of the Worm Wheel by TCA

a) meshing b) the three connected teeth

Figure 3
Tooth connection of the elements

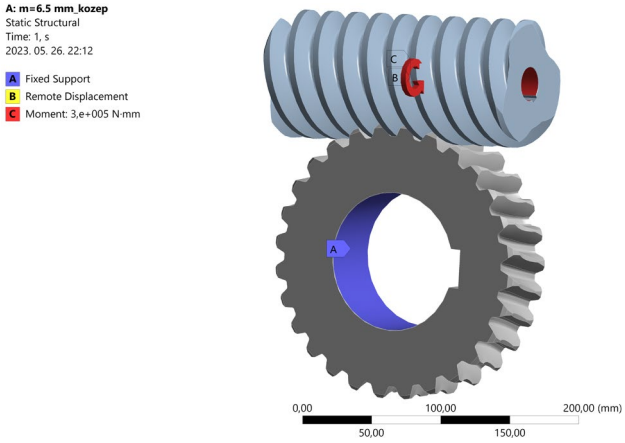

Figure 4
Tooth connection of the elements

Based on the geometrical facts, three worm wheel teeth are connected with the worm at the same time. Each connected tooth is analyzed. The material type of the elements is structural steel [28]. Dense meshing is applied on the analyzed contact

area (Figure 3). The dimension of the element is 0.4 mm. The method is tetrahedrons. Automatic meshing is selected on the outside area. The number of the nodes is 1133014. The number of the elements is 821968. The friction coefficient is $\mu=0.01$ on the contact zone. We suppose low friction between the contact surfaces (worm and worm gear). All degrees of freedom are fixed on the worm wheel. The rotation around the axis of rotation of the worm is permitted, other degrees of freedom are also fixed. The worm is loaded by 300 Nm torque around the axis of rotation. The same load is used for all of the drives (Figure 4).

4.1 Normal Stress Analysis

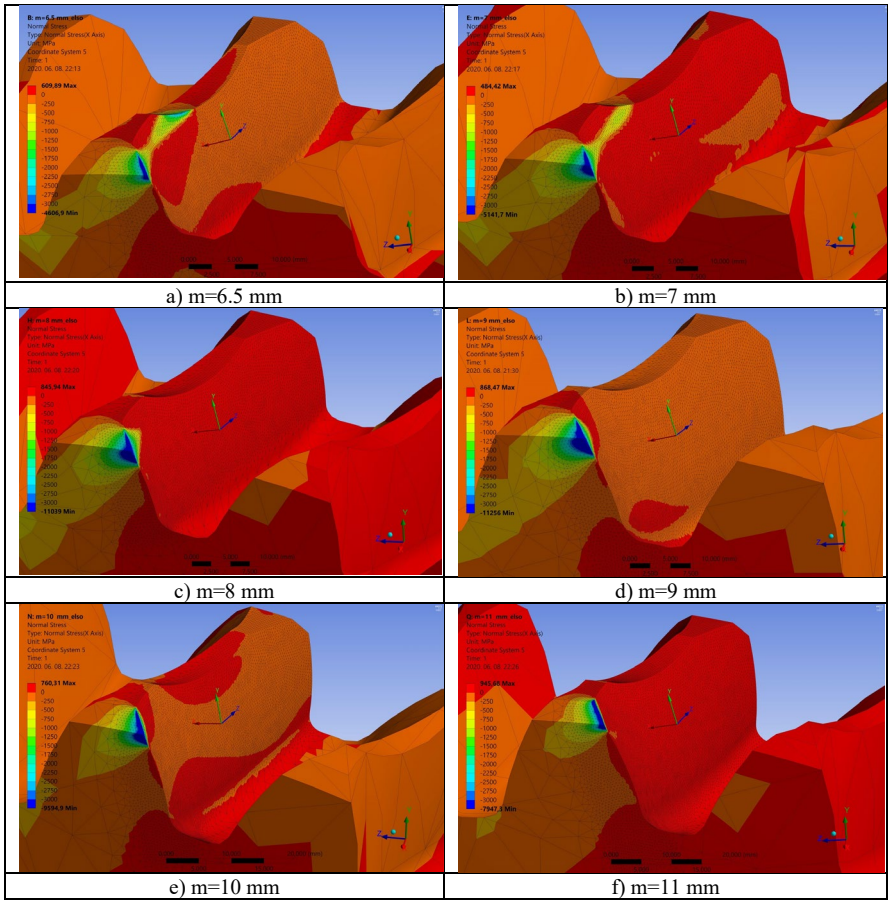

a) m=6.5 mm | b) m=7 mm

c) m=8 mm | d) m=9 mm

e) m=10 mm | f) m=11 mm

Figure 5
Normal stress results on the 1st tooth

The normal stress is interpreted perpendicularly for the surface of the worm wheel [19] [28]. We analyze the average stress results and the geometrical shape of the impressions on the surfaces of the worm wheels for each connected tooth. The result

on the 1st tooth can be seen on Figure 5. The received contact impressions on the teeth of the worm gears are approached by a lot of peripheral points which are imported to the GeoGebra mathematical software which is a complex mathematical software having a lot of operation possibilities. Using of this software, polygons were inserted at the imported peripheral points. As a result, we attained planar figures, that have areas and perimeters. They can be then calculated, for the comparisons. Figure 6 shows these polygons.

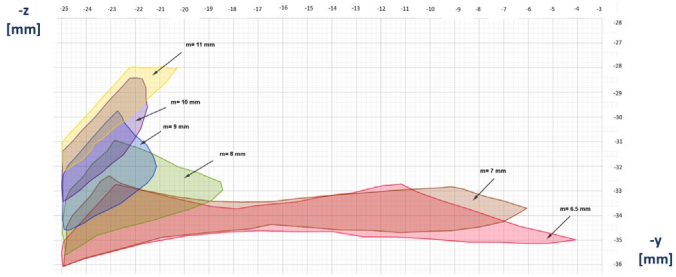

Figure 6
The structure of the stress impressions on the 1st tooth

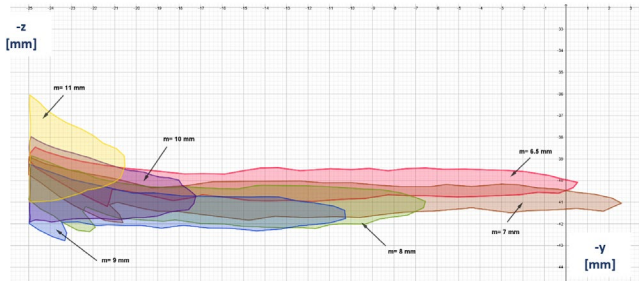

Figure 7
The structure of the stress impressions on the 2nd tooth

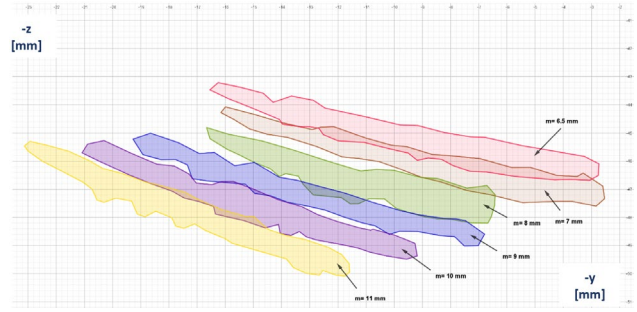

Figure 8
The structure of the stress impressions on the 3rd tooth

Result of the normal stress on the 2nd tooth can be seen on Figure 7. Figure 8 shows the results of normal stress on the 3rd tooth.

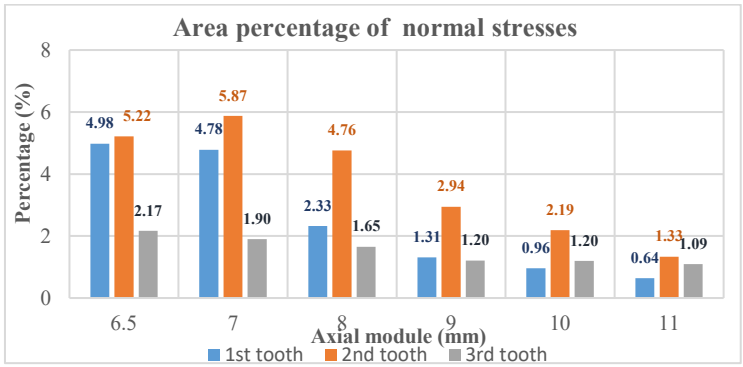

Figure 9

The area percentages of the impressions of the normal stress

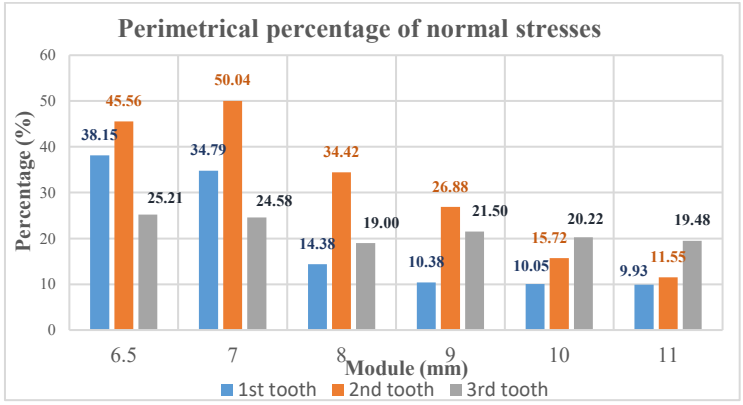

Figure 10

The perimetrical percentages as a result of the normal stress

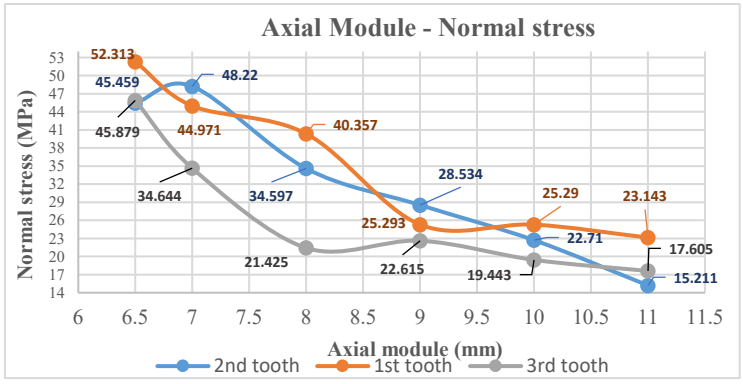

Figure 11

The average normal stress results in the function of the axial module

The geometrical areas of the surfaces of the worm wheels are determined by polygon method. Figure 9 shows the comparison of the contact impressions and the areas of the surfaces of the worm wheels in percentage.

Figure 10 shows the perimetrical percentages for the three teeth on each worm wheels as a result of the normal stress. The correlation between the average normal stress and the axial module can be seen in Figure 11.

4.2 Normal Deformation Analysis

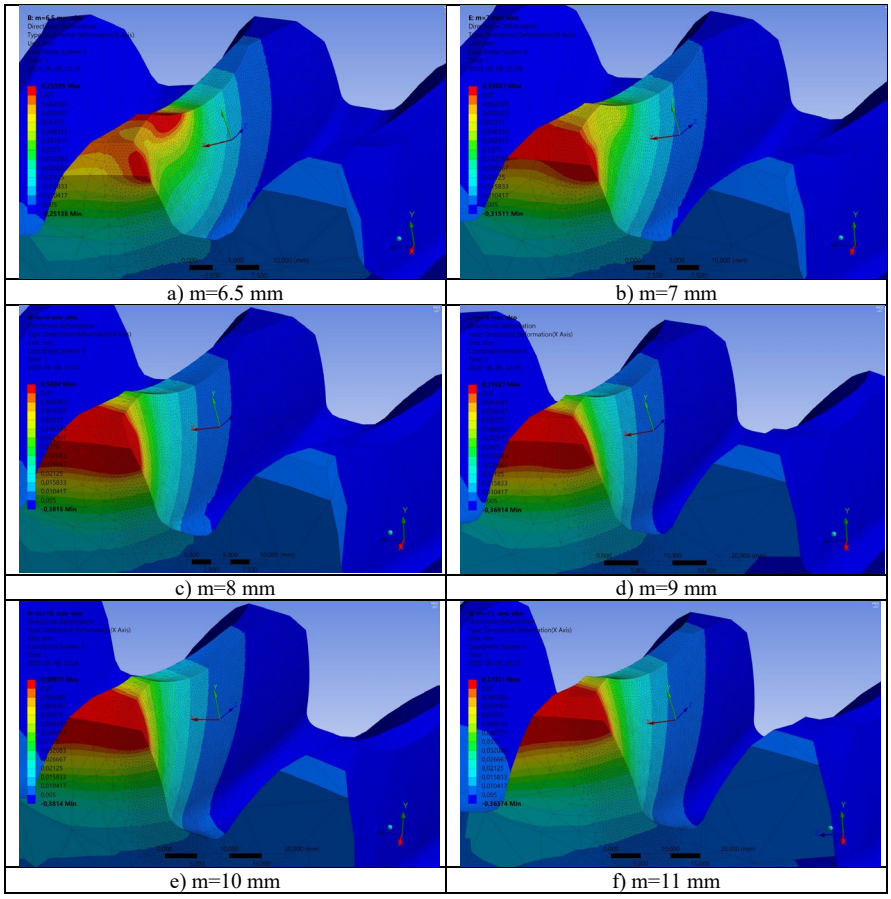

a) m=6.5 mm | b) m=7 mm

c) m=8 mm | d) m=9 mm

e) m=10 mm | f) m=11 mm

Figure 12

Results of normal deformation on the 1st tooth

The normal deformation is analyzed perpendicularly to the surface of the worm wheel [19] [28]. It was also analyzed for each connecting tooth of the worm wheel. The effects of the deformation zones are saved into the GeoGebra software. We approach the shape of the zones by lines which connect the border points of the

deformation zones (Polygon method). Similarly, to the stress analysis, we receive polygons, of which area and perimeter can be calculated. Figures 12 and 13, show the results for the case of the 1st tooth.

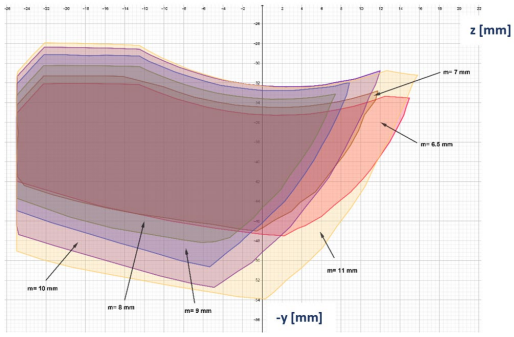

Figure 13
The resulted structure of deformation in case of the 1st tooth

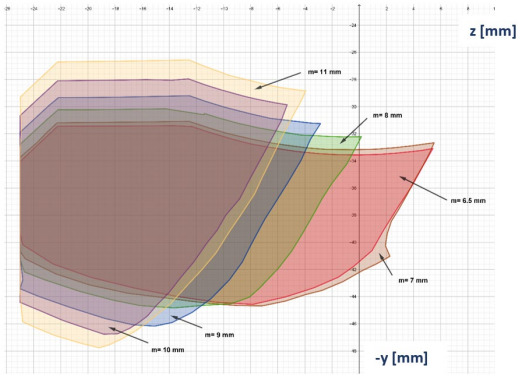

Figure 14
The structure of the deformation impressions on the 2nd tooth

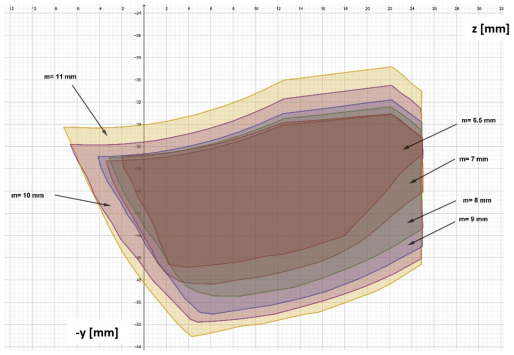

Figure 15
The scheme of the deformation impressions on the 3rd tooth

Figure 14 shows the result of the normal deformation in the 2nd tooth. Figure 15 shows the result of normal deformation in the 3rd tooth.

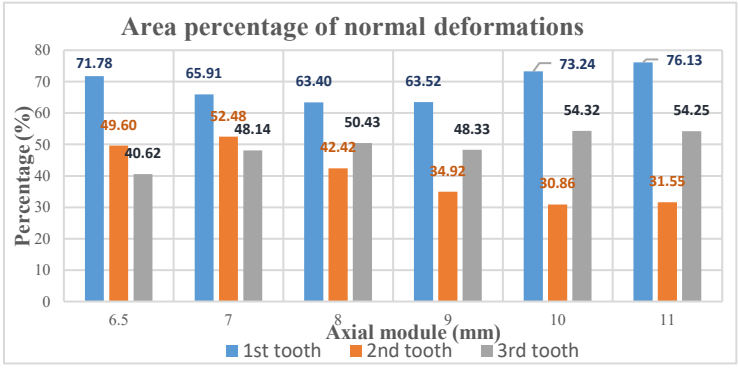

Figure 16

The resulted area percentages due to normal deformation

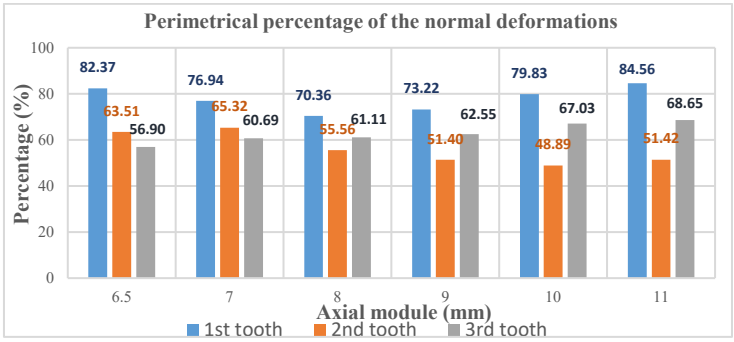

Figure 17

The resulted perimetrical percentages due to normal deformation

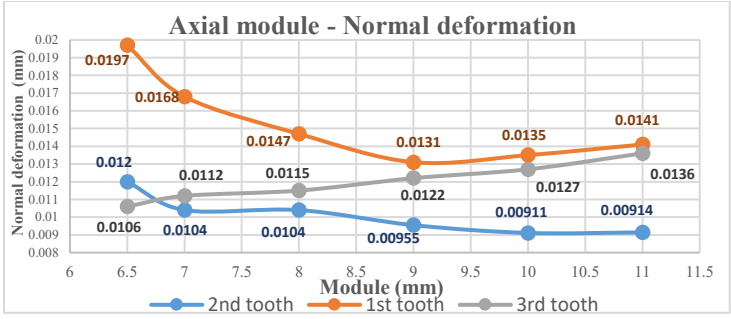

Figure 18

The average result due to normal deformation depending on the axial module

With the knowledge of the resultant areas, due to normal deformation and the whole surfaces of the teeth of the worm wheels, the area percentages can be determined (Figure 16).

Figure 17 shows the perimetrical percentages between the impressions of the normal deformations on the whole surfaces of the worm wheels.

The average normal deformation results in the function of the axial module, for each worm wheel, can be seen on Figure 18.

4.3 Axial- and Radial Deformation Analysis

The average deformations on the connecting teeth are also determined into axial and radial directions on the surfaces of the worm wheels (Figures 19 and 20).

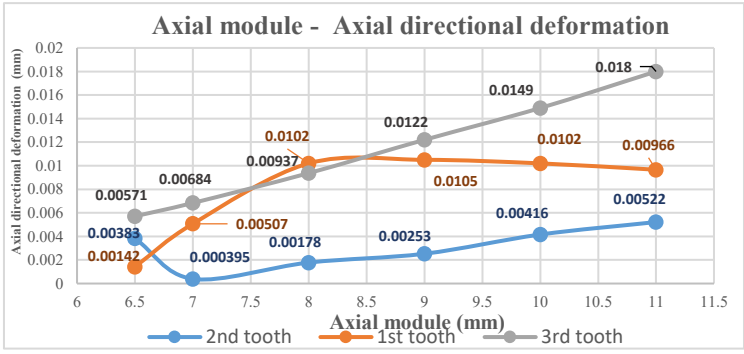

Figure 19

Axial module – axial directional deformation chart

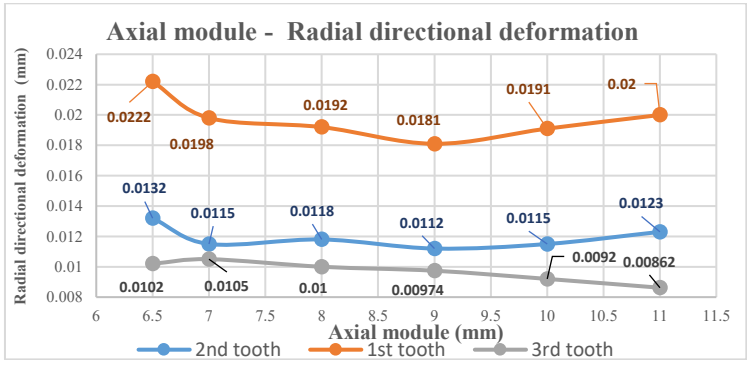

Figure 20

Axial module – radial directional deformation chart

Conclusions

The main property of the Archimedean worm is the linear profile, which is generated on the axial section of the worm, by a straight-lined blade. This geometry is widely used for different gear boxes providing good load transmission and high transmission ratio. That is why the TCA research is important, especially for their geometrical analysis. The mechanical parameters can be defined before the manufacturing and the real application.

The worm is loaded by 300 Nm torque around the axis of rotation in both cases. Analyzing the area percentages of the impressions (Figure 9) of the normal stress the following conclusions can be determined:

- The area percentages are continuously decreasing in the function of the enhancement of the axial module from m=7 mm axial module
- The highest percentages are on the 2nd tooth since it is totally in contact
- The results on the 3rd tooth are the lowest until the m=9 mm axial module
- After m=9 mm axial module the results on the 3rd tooth are higher than on the 1st tooth (m=10 mm and m= 11 mm)

Analyzing the perimetrical percentages of the normal stress (Figure 10) the following conclusions can be determined:

- The results are constantly decreasing as a function of the increase of the axial module
- The highest percentages are on the 2nd tooth until m=9 mm axial module
- After m=9 mm axial module that the highest results are on the 3rd teeth,
- The lowest results are on the 3rd tooth until m=7 mm axial module
- After m=7 mm axial module the lowest results are on the 1st teeth

Based on Figure 11, the average normal stress results are fluctuating and increasing depending on the increasing of the axial module. The lowest results are approximately on the 3rd tooth. The highest results on the 1st and 2nd teeth are always fluctuating depending on the axial module.

Analyzing the area percentages of the impressions (Figure 16) of the normal deformations the following conclusions can be determined:

- The highest results are received on the 1st tooth due to the maximum loads. This result decreases until the m=8 mm axial module. After that, it starts increasing
- The results for the 2nd and 3rd teeth are continuously fluctuating, depending on the axial module
- The percentage areas of the m=6.5 mm and m=7 mm axial module are higher on the 2nd tooth than on the 3rd tooth. After that, the results on the 3rd tooth are the second highest

Analyzing the perimetrical percentages of the impressions (Figure 17) of the normal deformations the following conclusions can be determined:

- The highest results are on the 1st tooth, which decreases until m=8 mm axial module. After that, the parameter of this tooth starts increasing
- The perimeter percentages of the m=6.5 mm and m=7 mm axial module of worm wheels are higher on the 2nd tooth, than on the 3rd tooth. After that, the results on the 3rd tooth are the 2nd highest
- The results on the 2nd tooth are continuously fluctuating depending on the axial module
- The results on the 3rd tooth are increasing depending on the axial module

The average normal deformation values are also calculated (Figure 18). The following conclusions can be determined:

- The highest results are received on the 1st tooth, which decreases until m= 9 mm axial module. After that, this parameter starts increasing. The highest result on the 1st tooth is in case of m=6.5 mm axial module
- The results on the 2nd tooth fluctuates and is continuously increasing. It is lower than the results on the 3rd tooth except in case of m=6.5 axial module
- The results on the 3rd tooth are continuously increasing depending on the axial module but it is always lower than the results on the 1st tooth

Based on the axial module – axial directional deformation chart (Figure 19) the following conclusions can be determined:

- The lowest results are on the 2nd tooth. It is continuously increasing form m=7 mm axial module
- The results on the 1st tooth are increasing until m=8 mm axial module. After that, they are decreasing. The highest result is in case of m=8 mm axial module
- The results on the 3rd tooth are continuously increasing depending on the axial module
- The results on the 3rd tooth are always higher than on the 2nd tooth

Based on the axial module – radial directional deformation chart (Figure 20) the following conclusions can be determined:

- The highest results are on the 1st tooth. This function is fluctuating. The highest result is in case of m=6.5 mm axial module
- The results of the 2nd tooth are also fluctuating. The highest results are in case of m=6.5 mm axial module
- The results of the 3rd tooth are continuously decreasing from m=7 mm axial module
- The lowest results are on the 3rd tooth

After the evaluation of the results, the geometric design of an Archimedean worm gear drive, is a very complex task. In this study, we analyzed the effects of the modification of the axial module, for the mechanical parameters, on the teeth of the worm wheels. We also shown the area and perimetrical percentages, for each tooth of the worm gear, in the function of the axial module. Our aim was to investigate the modification of the axial module, for the tooth contact zone and determine the dimensions of the tooth contact zone on the teeth of the worm gear. The wider the tooth connection zone, the better the power transmission at the teeth.

Acknowledgements

This research was supported by the **János Bolyai Research Scholarship of the Hungarian Academy of Sciences.**

Dr. Sándor Bodzás one of the authors of this publication, would like to express his great respect to **Prof. Illés Dudás † (2021)** (University of Miskolc, Miskolc, Hungary) who encouraged him and provided many consultations on the reasearch topic of worm gear drives. Prof. Dudás had several publications, scientific books and broad experience in this topic. He was the research leader of Dr. Sándor Bodzás' Ph.D. dissertation that was written in the field of geometric design and manufacturing analysis of conical worm gear drives and supported his work by useful remarks.

Dr. Sándor Bodzás, one of the authors of this publication, would like to express his great respect to **Prof. Tibor Bercsey † (2020)** (Budapest University of Technology and Economics, Budapest, Hungary) who provided many consultations on the reasearch topic of worm gear drives. Prof. Bercsey had several publications and broad experience in this topic. He was one of the reviewers of Dr. Sándor Bodzás' Ph.D. dissertation and supported his work by useful remarks.

References

[1] Zs. Balajti: *Development of production geometry of kinematical gear drives,* Ph.D. dissertation, Miskolc, University of Miskolc, 2007

[2] T. Bercsey: *Connection analysis of globoid worm and cylindrical gear having planar tooth surface,* University doctoral dissertation, Budapest, 1971

[3] T. Bercsey: *Theorem of toroidal drives*, Candidate dissertation, Budapest, 1977

[4] I. Dudás: *The Theory and Practice of Worm Gear Drives,* Kogan Page US., USA, 2004

[5] P. Horák: *Tribology analysis of worm gear drives having circular profile,* PhD dissertation, BME, Budapest, 2003

[6] F. L. Litvin: *Gear geometry and applied theory,* Englewood Cliffs, Prentice Hall, NJ., 1994

[7] F. L. Litvin, A. Fuentes: *Gear Geometry and Applied Theory,* Cambridge University Press, 2004, ISBN 978 0 521 81517 8

[8] I. Sz. Krivenko: *New Types of Worm Gears on Ships,* Sudostroenie, Leningrád, 1967

[9] C. Bolos, M. Ciotea, B. Bucur, V. Bolos: *Modeling the double worm-face gears,* Journal of Industrial Design and Engineering Graphics, Volume 10, 2015

[10] M. V. Chernets: *Prediction Method of Contact Pressures, Wear and Life of Worm Gears with Archimedean and Involute Worm,Taking Tooth Correction into Account,* Journal of Friction and Wear, 2019, Vol. 40, No. 4, pp. 342-348, ISSN 1068-3666, DOI: 10.3103/S1068366619040032

[11] K. Kawasaki, I. Tsuji: *Machining method of large-sized cylindrical worm gears with Niemann profiles using CNC machining center*, the International Journal of Advanced Manufacturing Technology, 2019, 104:3717-3729, https://doi.org/10.1007/s00170-019-04076-4

[12] J. Shon, N. Park: *Study on the influence of gear hobbing and shaft misalignments on the geometric interference of cylindrical worm gear set,* Journal of Mechanical Engineering Science, 2016, DOI: 10.1177/0954406216671543

[13] V. Goldfarb, N., Barmina: *Theory and Practice of Gearing and Transmissions,* Springer, 2016, p. 450, ISBN 978-3-319-19740-1, DOI 10.1007/978-3-319-19740-1

[14] V. Goldfarb, E. Trubachev, N. Barmina: *Advanced Gear Engineering,* Springer, 2018, p. 497, ISBN 978-3-319-60398-8, DOI 10.1007/978-3-319-60399-5

[15] Q. Meng, Y. Zhao, J. Cui, Z. Yang: *Meshing theory of mismatched ZC1 worm drive,* Mechanism and Machine Theory, Elsevier, 2020, https://doi.org/10.1016/j.mechmachtheory.2020.103869

[16] V. Vullo: *Gears, Volume 1: Geometric and Kinematic Design*, Springer, 2020, p. 880, ISBN 978-3-030-36501-1, https://doi.org/10.1007/978-3-030-36502-8

[17] J. Sohn, N. Park: *Geometric interference in cylindrical worm gear drives using oversized hob to cut worm gears*, Mechanism and Machine Theory, Elsevier, 2016, http://dx.doi.org/10.1016/j.mechmachtheory.2016.02.002

[18] Z. Zeng, Y. Chen, B. Chen, X. Du, C. Li: *Meshing performance investigations on a novel point-contact hourglass worm drive with backlash-adjustable*, Mechanism and Machine Theory, Elsevier, 2020, https://doi.org/10.1016/j.mechmachtheory.2020.103841

[19] S. Moaveni: *Finite Element Analysis, Theory and Application with ANSYS*, Pearson Education Limited, 2015, ISBN 10: 0-273-77430-1, p. 928

[20] Z. Terplán: *Machine elements IV.*, manuscript, Tankönyvkiadó, Budapest, 1975, p. 220

[21] S. P. Radzevich: *Dudley's Handbook of Practical Gear Design and Manufacture*, Third edition, CRC Press, 2016, p. 656, ISBN 9781498753104

[22] L. Dudás: *Modelling and simulation of a new worm gear drive having point-like contact, Engineering with Computers*, 2012, Engineering with Computers: Volume 29, Issue 3, 2013, pp. 251-272, ISSN 0177-0667

[23] F. L. Litvin, I. Gonzalez-Perez, K. Yukishima, A. Fuentes, K. Hayasaka: *Design, simulation of meshing, and contact stresses for an improved worm gear drive,* Mechanism and Machine Theory, Elsevier, Volume 42, Issue 8, 2007, pp. 940-959, https://doi.org/10.1016/j.mechmachtheory.2006.08.005

[24] T. Nieszporek, R. Gołębski, L. Soos: *Analysis of the worm-wheel toothing accuracy*, Technical Gazette, 24(4), 2017, 993-1000, https://doi.org/10.17559/TV-20160422094400

[25] S. Bodzás: Connection analysis of conical worm-, face gear- and tool surfaces, PhD dissertation, University of Miskolc, 2014, p. 154

[26] K. Bányai: *Inspection and production geometry of cylindrical worm gears,* University Doctoral Dissertation, Miskolc, 1977

[27] D. Maros, V. Killman, V. Rohonyi: *Worm gear drives,* Műszaki Könyvkiadó, Budapest, 1970

[28] S. Bodzás: *Computer-aided design and loaded tooth contact analyses of bevel gear pair having straight teeth by different loaded torques*, Mechanics & Industry 21 : 1 Paper: 109, 2020, https://doi.org/10.1051/meca/2019076

[29] J. Cui, Y. Zhao, Q. Meng, G. Li: *Calculation method for tooth thickness of cylindrical worm gear,* Forsch Ingenieurwes, 2021 https://doi.org/10.1007/s10010-021-00539-x

[30] A. B. Pop, A. M.Ţîţu: *Dynamic Simulation of Worm Gears Using CAD Applications.* In: Karabegović I. (eds) New Technologies, Development and Application IV. NT 2021. Lecture Notes in Networks and Systems, Vol. 233, Springer, Cham. https://doi.org/10.1007/978-3-030-75275-0_32

[31] B. Lu, Y. Chen, L. Shixuan, C. Bingkui: *Meshing performance investigations of involute worm and helical gear drive based on counterpart rack,* 2021*,* J Mech Sci Technol 35, 3533-3548, https://doi.org/10.1007/s12206-021-0725-7

Nomenclature

$\vec{v}_{1R}^{(12)}$	(mm/min^{-1})	Relative velocity vector
$\vec{n}_{1R}$		Normal vector of the surface in C_{1R} coordinate system
$\vec{r}_{1R}$		Placement vector of the moving points of the profile curve
$\vec{r}_P$		Position vector of the generating curve of the tool surface

$\boldsymbol{M_{1R,P}}$		Coordinate transformation matrix (transforms C_P to C_{1R})
O_{1R}, O_P		Origins of the appropriate coordinate systems
C_{1R} (x_{1R}, y_{1R}, z_{1R})		Rotational coordinate system related to the worm
C_P (x_P, y_P, z_P)		Tool coordinate system of generating curve
x, y, z	(mm)	Coordinates
η, $\boldsymbol{\theta}$		Internal parameters of the helicoidal surface
m_{ax}	(mm)	Axial module
p_d	(mm)	Diametral pitch
p_{dn}	(mm)	Normal diametral pitch
m_n	(mm)	Normal module
p_x	(mm)	Worm lead of thread
t_0	(mm)	Circular pitch of the worm-wheel
γ_m	(mm)	Lead angle
f’		Addendum coefficient
c*		Clearance coefficient
r’		Fillet coefficient
z_1		Number of threads
z_2		Number of teeth of the worm-wheel
d_{01}	(mm)	Pitch diameter of the worm
d_{02}	(mm)	Pitch diameter of the worm-wheel
d_{a1}	(mm)	Outside diameter of the worm
d_{a2}	(mm)	Outside diameter of the worm-wheel
a	(mm)	Center distance
b_2	(mm)	Face width of the worm-wheel
L	(mm)	Worm length
α_{ax}	(°)	Pressure angle
α_n	(°)	Normal pressure angle
h_{a1}	(mm)	Addendum of the worm
h_{a2}	(mm)	Addendum of the worm-wheel
h_{f1}	(mm)	Dedendum of the worm
h_{f2}	(mm)	Dedendum of the worm-wheel
S_{ax1}	(mm)	Tooth thickness of the worm
S_{ax2}	(mm)	Tooth thickness of the worm- wheel
r	(mm)	Fillet radius
j	(mm)	Backlash
i		Transmission ratio
q		Diameter ratio
M	(Nm)	Load torque
μ		Friction coefficient
TCA		Tooth Contact Analysis
CAD		Computer Aided Design